

Impedance Response Analysis of Anion Exchange Membrane Electrolyzers for Determination of the Electrochemically Active Catalyst Surface Area

Sebastian A. Watzele,^[a, b] Regina M. Kluge,^[a] Artjom Maljusch,^[b] Patrick Borowski,^[b] and Aliaksandr S. Bandarenka^{*[a, c]}

Polymer membrane electrolyzers benefit from high-pressure operation conditions and low gas cross-over and can either conduct protons (H^+) or hydroxide ions (OH^-). Both types of electrolyzers have a similar design, but differ in power density and the choice of catalysts. Despite the significant endeavor of their optimization, to date, there is no well-established impedance model for detailed analysis for either type of these devices. This complicates the *in-situ* characterization of electrolyzers, hindering the investigation of degradation mechanisms and electrocatalytic processes as a function of applied current density or time. Nevertheless, a detailed understanding of such individual processes and distinguishing the performance-limit-

ing factors are the keystones for sophisticated device optimization. In this work, an impedance model based on electrode processes has been developed for an anion exchange membrane electrolyzer utilizing iridium oxide anode and platinum cathode electrocatalysts. This model allows to deconvolute the measured impedances into constituents related to the individual electrode processes and to estimate actual physico-chemical quantities such as the reaction kinetic parameters and double-layer capacitances. We discuss the meaning of the fitting parameters and show that this model enables, for the first time, the estimation of the electrochemically active surface area of the anode electrocatalysts under reaction conditions.

Introduction


Hydrogen is not only attractive for energy storage; it is also a valuable feedstock for chemical synthesis, e.g., with CO as syngas, but also needed for fertilizer production and steel refining.^[1,2] At present, the major fraction of hydrogen is still produced from fossil fuels.^[3] However, there is an increasing interest in electrochemical synthesis, not only due to climate awareness but also due to rising natural gas prices.^[4–7] In low-temperature water electrolysis, alkaline and proton exchange membrane (PEM) electrolysis are the main technologies.^[3] The former achieves relatively low current densities, but can dispense with the use of precious metal catalysts. PEM technology, on the other hand, allows higher production rates and a more compact design, but requires a considerable amount of precious-metals catalyst.^[3] As a result, the anion


exchange membrane (AEM) electrolyzer has attracted much attention recently. It uses a similar cell design to classical PEM electrolysis. However, by using a membrane permeable to anions, an alkaline environment can be created in which platinum-group metal (PGM)-free catalysts can be used.^[8,9] However, these AEMs suffered from low conductivities or low long-term stability until very recently.^[8] With the commercialization of highly conductive and stable anion exchange membranes, the AEM technology will combine the advantages of the two technologies mentioned above to produce compressed hydrogen with comparable power density and efficiency to PEM electrolyzers but without the use of precious metal-containing components.^[8] However, the critical step to successful implementation is the optimization of the AEM electrolysis units and their optimal combination. Optimization requires detailed knowledge of the processes and conditions at the anode and cathode catalyst layers as well as the membrane. Indeed, the reactions occurring at the anode and cathode, namely the oxygen (OER) and hydrogen evolution reaction (HER), are well known. However, it is generally hard to differentiate and quantify the losses at the anode, cathode, membrane, and liquid gas diffusion layers, especially under reaction conditions. Determining the losses and their origin is crucial to systematically improving an electrolyzer.^[10] For example, the limited performance of the anode can be due to many factors, such as catalyst distribution, catalyst activity, limited active surface area, or poor electrolyte management.^[11,12] Unfortunately, certain essential phenomena can only be monitored under reaction conditions. However, typical *in-situ* analyses are limited to the investigation of voltage-current characteristics and determining high-frequency cell resistance.

[a] Dr. S. A. Watzele, Dr. R. M. Kluge, Prof. Dr. A. S. Bandarenka
Physics of Energy Conversion and Storage, Department of Physics, Technical University of Munich, James-Franck-Straße 1, 85748, Garching, Germany
E-mail: bandarenka@ph.tum.de

[b] Dr. S. A. Watzele, Dr. A. Maljusch, P. Borowski
Evonik Operations GmbH, Paul-Baumann-Straße 1, 45772, Marl, Germany

[c] Prof. Dr. A. S. Bandarenka
Catalysis Research Center TUM, Ernst-Otto-Fischer-Str. 1, 85748, Garching, Germany

 Supporting information for this article is available on the WWW under <https://doi.org/10.1002/cmt.202300035>

 © 2024 The Authors. Chemistry - Methods published by Chemistry Europe and Wiley-VCH GmbH. This is an open access article under the terms of the Creative Commons Attribution License, which permits use, distribution and reproduction in any medium, provided the original work is properly cited.

In some cases, the charge transfer resistance is also determined using electrochemical impedance spectroscopy (EIS) using largely empirical fit models.^[13–16] However, the meaning of the constituents of the model and, thus, quantitative determination of important physico-chemical parameters is usually not possible. Certain scientific work has attempted to fit the impedance spectra by using combinations of constant phase elements and resistors. This improves the fitting at the cost of little meaning of most of the fitting parameters.

In this work, a novel impedance model was developed that allows a more accurate analysis of the measured impedances, taking into account the individual electrodes and thus allowing real physical quantities such as the reaction kinetic parameters and double-layer capacitances of cathode and anode to be studied separately. The estimation of the electrochemically active surface area of the anode electrocatalysts under reaction conditions is also discussed.

Results and Discussion

Briefly, separate electrochemical models for the anodic and cathodic half-cells were used and combined to create the AEM membrane-electrode assembly (MEA) model. The impedance of separate electrodes includes the uncompensated resistance and the parts related to the non-Faradaic processes and Faradaic parts (see Figures 1A and 1B), which represent the stages of the interfacial charge transfer. In the next paragraph, the modeling of both the cathode and anode is considered, and the constituents are explained separately. Later on, a model for the whole AEM MEA is composed and discussed. The informative power of this model will be demonstrated in determining physical quantities, taking the example of estimating the electrochemically active surface area (ECSA) of the anode catalyst under reaction conditions.

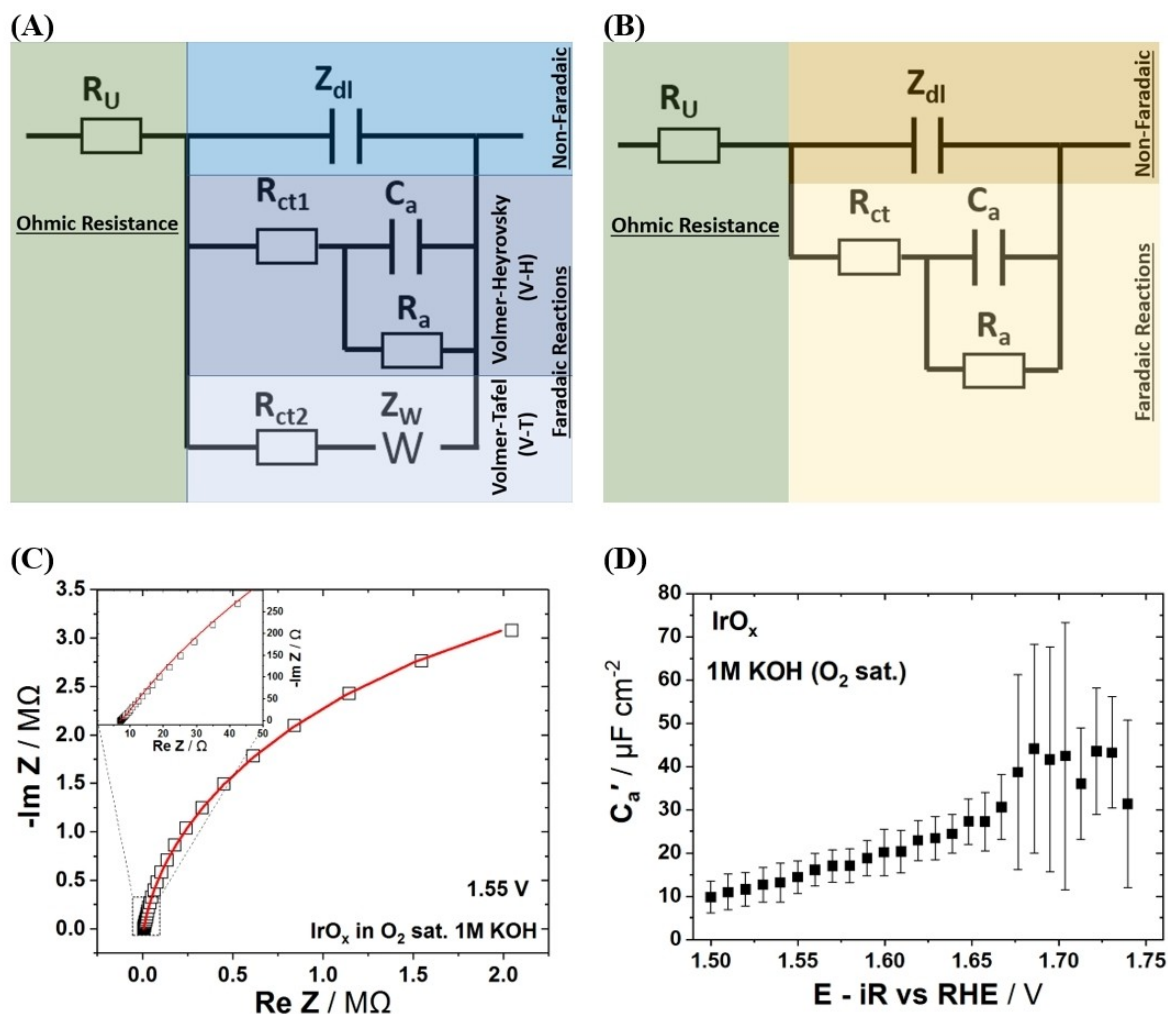


Figure 1. (A,B) Equivalent circuit for (A) the cathodic and (B) the anodic half-cell. (C) A typical example of the spectrum and the fitting results for the anode material grown on the surface of Ir(111). (D) The dependence of the adsorption capacitance for the Ir-oxide electrode on the potential. See the text for the explanation.

Modeling using the equivalent circuit of the cathode

The equivalent electrical circuit (EEC) for the cathode is given in Figure 1A. Here, the capacitive non-Faradaic branch (related to the double layer response) is modeled with a constant phase element or capacitor. For the Faradaic constituent, individual reaction mechanisms are to be considered. The HER can occur at the cathode *via* the Volmer-Heyrovsky (V-H) and Volmer-Tafel (V-T) pathways. A proton already adsorbed on the catalyst surface in the V-H pathway reacts with another proton approaching from the electrolyte side. In the case of an alkaline electrolyte, a water molecule dissociates, and the released proton reacts with the already adsorbed proton, exchanging the charge with the solid electrode. Linearizing the AC impedance response equation, it can be graphically represented as a charge transfer resistance in series with an adsorption capacitance in the EEC, which in turn is parallel to an adsorption resistor.^[17,18] In Figure 1A, the V-H pathway corresponds to the second branch. For the derivation, please refer to the literature.^[18] In the V-T pathway, two surface-adsorbed protons recombine to form a hydrogen molecule without additional charge transfer during the combination step. Therefore, the reaction in the last step is diffusion-limited. The associated EEC consists of a charge transfer resistance in series with a semi-infinite Warburg element.^[18] It is given as the third branch in Figure 1A. Since V-H and V-T are parallel reactions, the corresponding EECs are also in parallel. In our previous publication,^[18] we showed that the contribution of the individual pathways to the overall reaction rate could be estimated by comparing the corresponding charge transfer resistances.^[18]

Modeling using the equivalent circuit of the anode

The EEC of the anode is shown in Figure 1B. Here, one also finds the uncompensated resistance R_U and a similar non-Faradaic branch as in the case of the cathode. Considering the Faradaic branch, the OER is more complex due to multiple adsorption steps, making optimal catalyst design difficult with suitable adsorption energies for all intermediates.^[19] However, as shown in previous work,^[20,21] the impedance spectra do not usually exhibit specific features. It can be concluded that only one adsorption step is crucial, which, analogous to the V-H pathway at the cathode, can be represented by charge transfer, adsorption capacitance, and resistance. This is shown as the second branch in Figure 1B.

Calibration measurement for the electrochemically active surface area determination of the anode

It is crucial to mention the particular importance of the adsorption pseudo-capacitance in the model of the anode. Recently, it was shown that this parameter is suitable to determine the ECSA of an OER catalyst.^[26] For the ECSA determination, the adsorption capacity is obtained from the EIS analysis as a fit parameter and subsequently divided by the

adsorption capacity specific to the material and electrolyte (C_a'): $ECSA=C_a/C_a'$. By now, there is a small database of material-specific adsorption capacities that includes IrO_x in different electrolytes.^[21] However, since the corresponding specific adsorption capacity of IrO_x in 1 M KOH has not yet been determined, this will be done first. For this purpose, impedance spectra between 1.50 V and 1.75 V were recorded of a known iridium oxyhydroxide surface ($\sim 0.196 \text{ cm}^2$)^[22,23] in 1 M KOH and fitted using the EEC shown in Figure 1B. As seen in the representative fit shown in Figure 1C, the entire impedance spectrum between 30 kHz and 0.1 Hz can be modeled with the selected EEC for the anode. The adsorption capacities determined from the fits and the standard deviation from at least four measurements each can be plotted *versus* the applied potential in Figure 1D. It is striking that the specific adsorption capacity increases with increasing potential, coinciding with earlier observations for IrO_x in 0.1 M KOH.^[26] For the later estimations of anode catalyst ECSA, note the reference value of $C_a'(1.56 \text{ V}) \sim 17 \mu\text{F cm}^{-2}$.

Modeling and discussion of the equivalent circuit of the anion-exchange-membrane electrode assembly

In the following, we elaborate on the MEA of an anion exchange membrane electrolyzer and the composite fitting model. In Figure 2, a sketch of the individual constituents of the electrolyzer is given. We derived an EEC, which includes the individual building blocks validated previously as impedance models. For a better overview, the AEM MEA is discussed from left to right in Figure 2, first. The meaning of the elements of the EEC is discussed afterward.

On the left side of Figure 2 is the (liquid) gas diffusion layer (L)GDL, which consists of a porous conductive material that allows both water and oxygen to be transported to the flow plate (not shown in this schematic). In addition, this layer provides the electrical connection between the catalyst layer and the anodic flow plate. The anode catalyst layer (ACL) catalyzes the OER. Since the experiment is for demonstration purposes, a commercially available iridium-based catalyst was used because of its long-term stability and high reproducibility. In general, of course, the use of a PGM-free catalyst is preferable due to its lower price. But the elaborated model can easily be adapted to any OER catalyst. The catalyst particles are embedded in an ionomer matrix to improve ionic conductivity and mechanical properties. The heart of any alkaline MEA unit is the anion-conducting membrane, which provides ionic conductivity and, in limited amounts, water transport, but separates the gas phases. The structure of the cathode side (further right) resembles the design of the anode. However, the catalyst layer uses platinum on carbon. The carbon is largely inactive and serves only to maximize the active Pt surface and improve the conductivity. The gas diffusion layer (GDL), which can be hydrophobized if desired to reduce the cathodic water content, ensures electronic contact with the flow plates.

The elements of the EEC can be assigned to the anode and cathode and are related to the individual physico-chemical

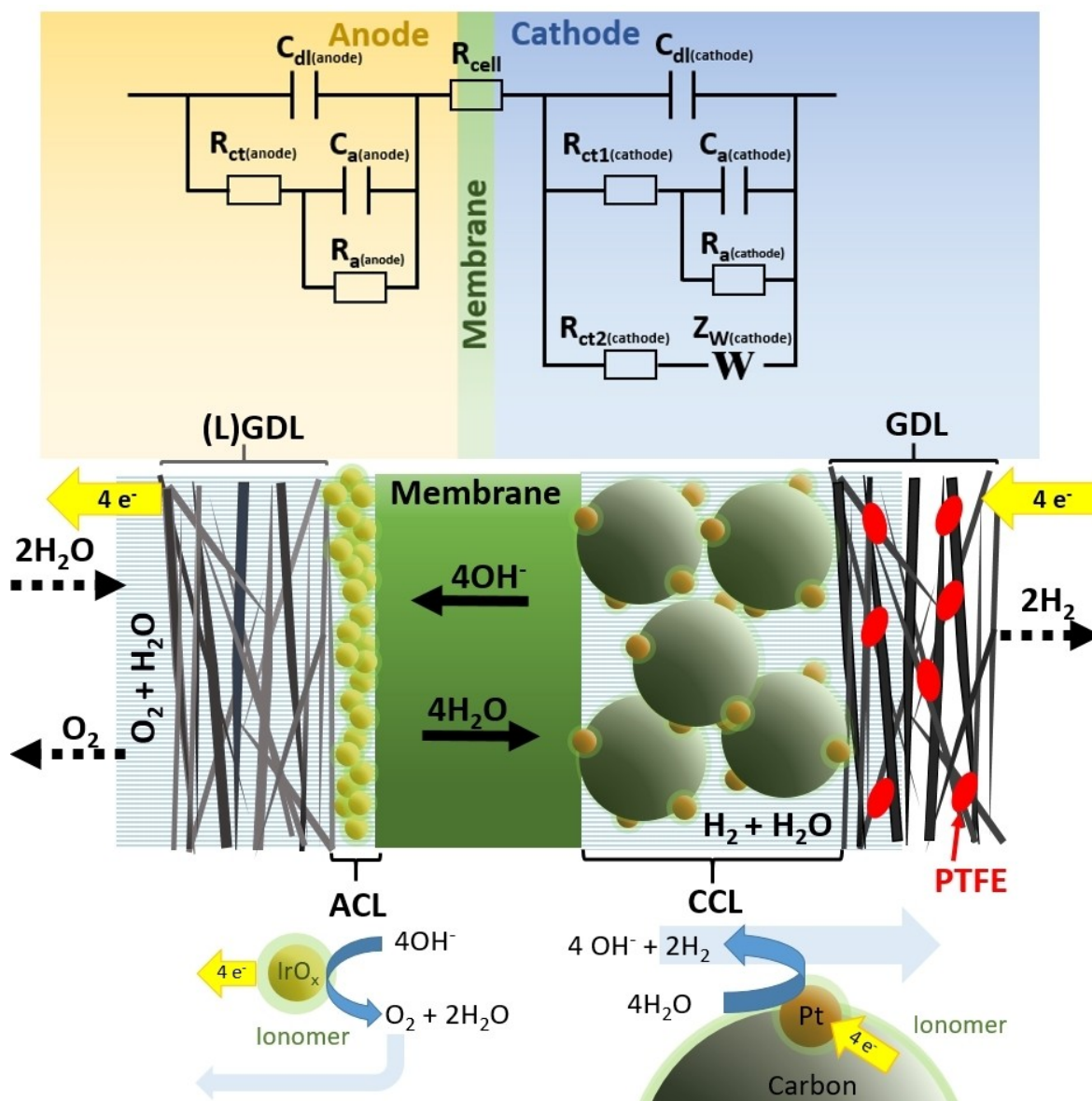


Figure 2. Sketch of an AEM MEA with the corresponding EEC. The MEA consists of an OH^- conducting membrane, which is on both sides in contact to a catalyst layer. The anode catalyst layer (ACL) consists of IrO_x nanoparticles with an ionomer binder ensuring mechanical stability and OH^- ion conductivity. The CCL promotes the HER, forming hydrogen molecules and OH^- ions from water. The EEC results from the combination of the anodic (Figure 1B) and cathodic (Figure 1A) half-cell. More details on the model are given in the main text.

parameters. As a basic constituent, there is a cell resistance R_{cell} , often also called high-frequency resistance, which includes the membrane resistance, average resistance of the ionomer, and electronic resistances, e.g., in the gas diffusion layer and contact resistances. There are both anodic and cathodic double-layer capacitances. At constant temperature and for a given electrode material, they are approximately proportional to the surface area of the electrodes. Since the cathodic catalyst layer has a higher surface area due to the carbon support, this should be reflected in the cathode's comparatively larger double-layer capacitance. The two parallel charge transfer resistances give the cathodic charge transfer. Comparing $R_{\text{ct1(cathode)}}$ with $R_{\text{ct2(cathode)}}$, it can be determined whether the V-H or the V-T mechanism dominates at the respective applied

current density. The cathodic adsorption capacity and the adsorption resistance are only of minor importance. They describe the change of the fractional adsorbate coverage with a change in the applied potential. The Warburg coefficient, on the other hand, has greater practical significance. If this increases, for example, with increased current density, this indicates a mass transfer limitation. This can be, e.g., a sign of dry running of the cathode due to insufficient water supply. On the anode side, there is only a charge transfer resistance, which, together with the adsorption resistance $R_{\text{a(anode)}}$, describes the potential change when the applied current density is modified. The anodic adsorption pseudo-capacitance is of special importance. It can be used to estimate the electrochemically active catalyst surface area (ECSA) during the operation of the cell,

which will be demonstrated later in this work. Note that the presented model does not account for pore resistances which can become dominating in systems with porous catalyst layers in the high frequency regime. A transmission line model as shown by Eikerling and Kornyshev^[24] and which has been further studied with physical models, by Kosakian,^[25] Secanell^[26] and Reshetenko,^[27] among others,^[28] can be in principle combined with the presented model. This modification can allow more accurate evaluation of impedance data especially in the high frequency regime. However, it comes at the price of a model with more free variables which requires almost artefact-free impedance data (especially in the high frequency regime) which is highly difficult to acquire at elevated current densities. Further, the effect of pores is more significant for systems with catalyst coated membranes which is briefly discussed in the supporting information.

Application and evaluation of the impedance model

The model described above was used to fit electrochemical impedance spectra recorded at current densities between 100 mA cm^{-2} and 1000 mA cm^{-2} in the range of about 10 kHz and 1 Hz. As seen in Figure 3 (and Figure S1), in this frequency range the spectra have low noise levels, and the EEC allows high-precision modeling for all recorded spectra in the entire frequency range. Relatively small root-mean-squared deviations and estimated individual parameter uncertainties indicate the significance of each element.

With the bare eye, it is only qualitatively noticeable that all spectra have approximately the same high-frequency resistance, consist of several overlapping semicircles and that the overall charge transfer resistance decreases towards higher current densities. However, the parameters acquired by the fit need to be examined for a more detailed analysis. The cell resistance, shown in Figure 4A, initially drops between 100 mA and 250 mA but saturates at higher currents. The improvement in

conductivity at higher current densities can be explained by factors such as compression of the cathodic catalyst layer by individual hydrogen bubble formation. Further, as expected, a decrease in the anodic charge transfer resistance and adsorption resistance can be observed. Looking at the anodic and cathodic double-layer capacitance shown in Figure 4B, two important observations can be made. First, the cathodic double layer capacitance is about one order of magnitude larger than that of the anode. This is due to the increased surface area of the cathode since the catalyst comprises high surface area carbon. Secondly, it can be seen that both capacitances decrease significantly with increasing current density. This is caused by oxygen and hydrogen gas formation at the anode and cathode, respectively. At higher current densities, the gas phase increases and displaces the alkaline electrolyte, resulting in a reduced electrode surface area in contact with the electrolyte.

Analyzing the cathodic charge transfer resistances shown in Figure 4C, it is noticeable that R_{ct2} decreases and R_{ct1} slightly increases towards higher current densities. Since R_{ct2} is initially higher, this indicates a dominant V-H pathway, although for 1000 mA cm^{-2} the trend is reversed in favor of the V-T pathway. The R_{ct} combined from both pathways decreases towards higher current densities, as expected. Figure 4D shows the anodic adsorption capacitance, which behaves analogously to the specific adsorption capacitance measured in Figure 1D and increases with increasing current density and potential. The electrochemically active surface area can be estimated according to $ECSA = C_a / C_a' = 0.82 \text{ F} / 17 \mu\text{F cm}^{-2} \sim 4.8 \text{ m}^2$. Comparable iridium catalysts are reported to have $\sim 21\text{--}60 \text{ m}^2 \text{ g}^{-1}$.^[29] Due to its lower density, the specific surface area significantly increases when iridium is converted to iridium oxide or oxyhydroxide. For instance, for IrO_x a BET (Brunauer-Emmett-Teller) surface area of $175\text{--}195 \text{ m}^2 \text{ g}^{-1}$ is typical.^[30] With a surface loading of 1 mg Ir cm^{-2} and a coated area of 25 cm^2 , a surface area of up to $\sim 4.6 \text{ m}^2$ can be estimated. This is in reasonable agreement with the electroactive surface area determined by the impedance

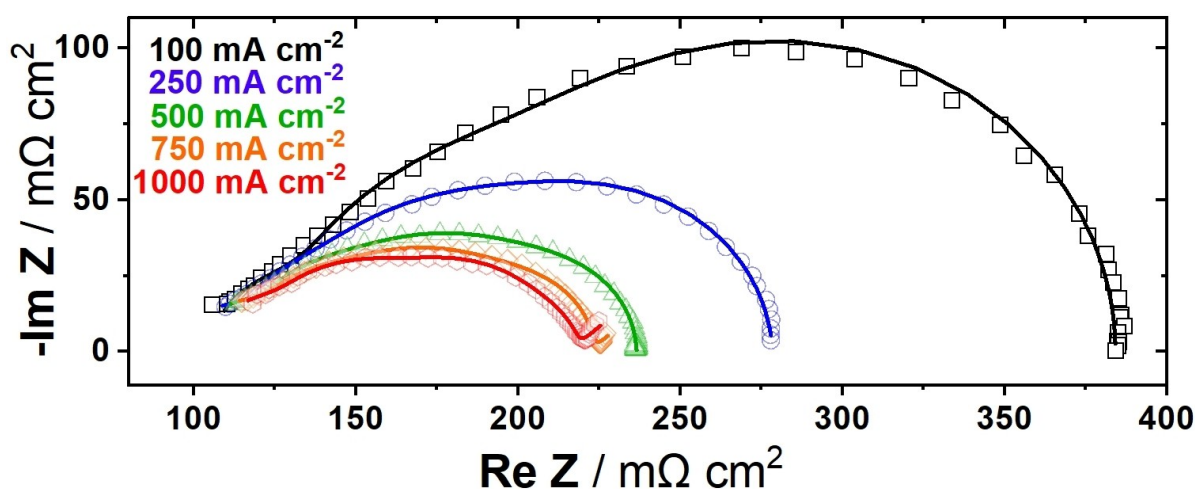


Figure 3. Representative EIS spectra recorded at current densities ranging from 100 mA cm^{-2} to 1000 mA cm^{-2} (open symbols). Corresponding fits (lines) are based on the EEC shown in Figure 2. All fits show only relatively small root-mean-squared deviations in a frequency range from 1 kHz to 1 Hz. Exemplary bode plots are shown in Figure S2.

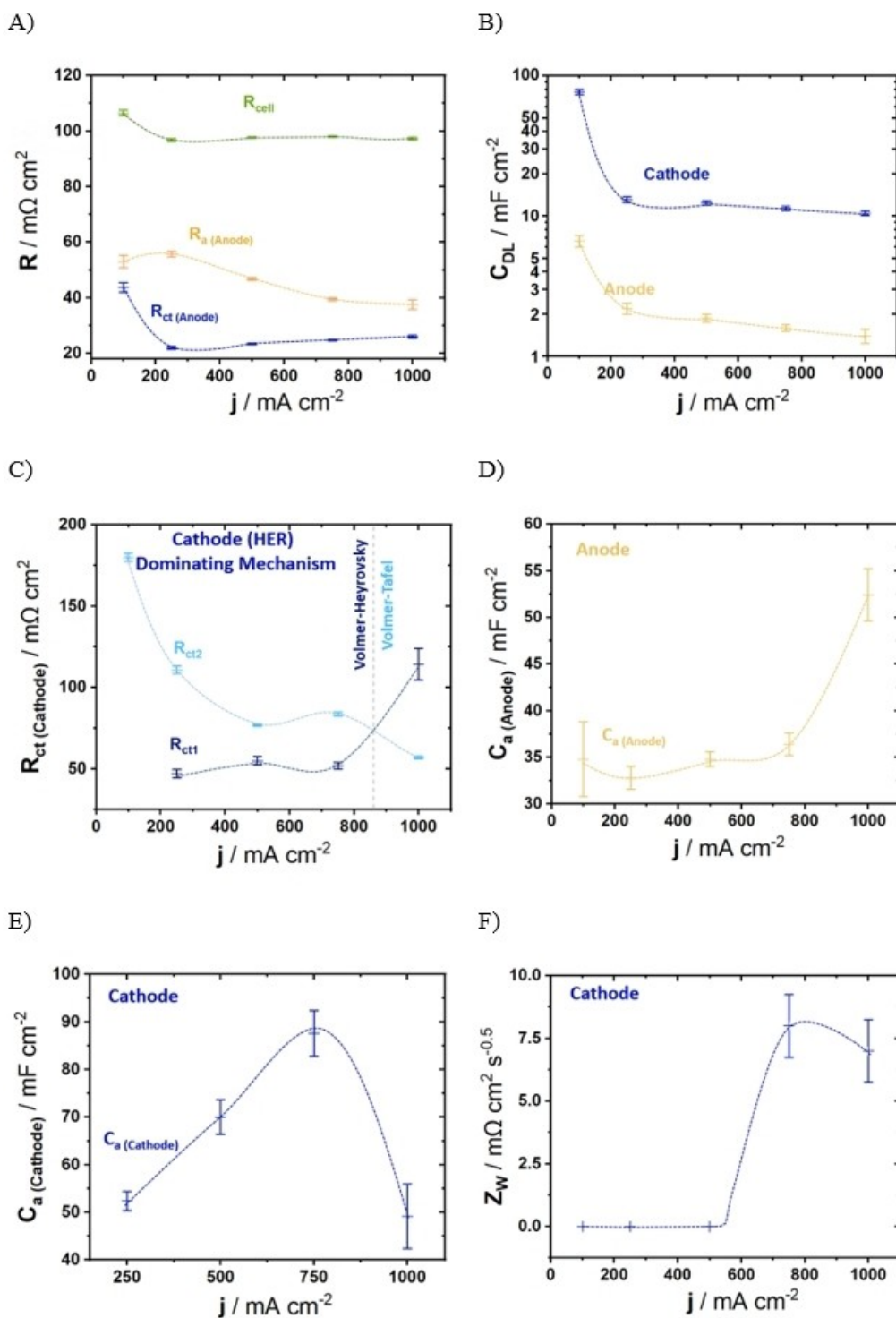


Figure 4. Individual fitting parameters of the EIS data, shown in Figure 3, as a function of the applied current density. The fitting parameters are represented with their corresponding error bars and the dotted lines are a guide to the eye. (A) Cell and anodic charge transfer and adsorption resistances. (B) Anodic and cathodic double-layer capacitance plotted in a semi-logarithmic scale. Both capacitances decrease with increasing current densities. However, the double-layer capacitance for the cathode is always significantly higher than for the anode (by a factor of ~6). (C) Charge transfer resistances of the cathodic half-cell reaction. $R_{\text{ct}1}$ and $R_{\text{ct}2}$ correspond to the Volmer-Heyrovsky and Volmer-Tafel reaction pathways, respectively. The graph indicates a transition from a dominating Volmer-Heyrovsky mechanism at low current densities toward a dominating Volmer-Tafel mechanism at high current densities. (D) Anodic adsorption capacitance. (E) Cathodic adsorption capacitance. (F) Fitting values of the (infinite) Warburg element in the Faradaic branch of the anode. Note that diffusion limitations were only detected for current densities exceeding 500 mA cm^{-2} .

analysis. The discrepancy is expected to be caused by an underestimation of the specific adsorption capacity during the

rotating disk electrode (RDE) measurements, as oxygen micro-bubbles may have adhered to the bottom of the RDE and thus

reduced the active surface area. To the best of our knowledge, our developed model allows for the first time to determine the electrochemically active surface of an electrolyzer anode under reaction conditions. The corresponding voltage current curve of the test cell is shown in Figure S2.

Having demonstrated the validity of our model for a commercial IrO_x catalyst, we point out that the model is not limited to this choice of material. We have recently shown that the anode model can be applied to a wide range of OER catalysts.^[21] The cathode adsorption capacitance plays only a minor role in comparison. As shown in Figure 4E, it increases until a current density of 750 mA cm⁻² and then decreases again, indicating maximum reversibility of the proton adsorption step at 750 mA cm⁻². The Warburg impedance is constant at zero for low current densities and is not required for the fit, as no diffusion limitation occurs. However, above 750 mA cm⁻² it becomes visible by the 45° bend in the impedance spectra at low frequency. This is easily explained since mass transport phenomena are typically identified only at comparatively high current densities. In this case, dry running of the MEA can be excluded since R_{cell} remains constant and would increase in case of dry running. Therefore, another mass transport phenomenon must be considered, such as hydrogen diffusion through the ionomer. For completeness, all fitting values are listed in the supporting information (see S1). As demonstrated, all fitting parameters of the EEC are based on real, (theoretically) measurable dimensions and allow actual statements about the electrochemical system of the AEM electrolyzer. This significantly improves the analysis and allows targeted optimization.

Crucial for the application of the EEC is a clean impedance spectrum of the stationary electrolysis system in a frequency range of at least 1 Hz to 1 kHz, better 0.1 Hz to 10 kHz with sufficient data points as well as a high signal-to-noise ratio. For the tested cell design the features in the frequency range between 50 Hz and 350 Hz showed major impact on the value of C_a. It is important to avoid measurement artifacts, e.g., due to unfavorable cable routing, and to check the recorded spectra, e.g., via Kramers-Kronig relation.

Conclusions

In this work, an impedance model for the analysis of the AEM electrolyzer EIS data was developed. The impedance spectra were analyzed at different current densities using the developed model. The fit parameters and their significance for the electrolyzer system were briefly, discussed and checked for plausibility. The anodic adsorption capacity was correlated with the electrocatalytically active surface area of the anode catalyst under operational conditions. The model significantly improves the analyzability of impedance spectra recorded for AEM electrolyzers.

Experimental Section

All chemicals were high-purity reagents and used as received. Ultrapure water was acquired by a filter machine (Evoqua, 18.2 MΩ cm, less than 5 ppb of total organic contamination). For all experiments, 1 M KOH served as the electrolyte, which was prepared from the KOH pellets (85% Sigma Aldrich, Germany) or bought as 1 M KOH solution (Sigma Aldrich) in case of calibration measurements for C_a determination or electrolyzer measurements, respectively.

For the calibration measurements, a three-electrode cell was used, and glassware was cleaned prior with Caro's acid and several times flushed with boiling, ultrapure water. A Pt wire (99.99% Mateck, Germany) and a Hg/Hg₂SO₄ (0.6 M K₂SO₄, Schott, Germany) electrode served as counter and reference electrodes, respectively. An Ir(111) disk electrode (Mateck, Germany) was used as the working electrode. The electrode surface was electrochemically oxidized, as shown elsewhere,^[31] resulting in a surface with a low roughness factor. Potentials were controlled by a VSP-300 potentiostat (Biologic, France), and all potentials were referred to *versus* the reversible hydrogen electrode (RHE) scale. EIS spectra were recorded in 10 mV steps, ranging from 30 kHz to 1 Hz, using a perturbation amplitude of 10 mV. A shunt capacitor of ~4 μF was connected between the reference electrode and an additional Pt wire which was set close to the tip of the Luggin capillary to suppress measurement artifacts in the high-frequency regime. For better comparability, the potentials were corrected by the voltage drop in the electrolyte, derived by the multiplication of the uncompensated resistance with the current density.

The electrolyzer MEA had an active area of 25 cm² and used an anion exchange membrane DURAION® (Evonik Operations GmbH, Germany) with a thickness of ~65 μm. Ir black (1 mg cm⁻²) and Pt/C (60% wt., 1 mg cm⁻²) served as anode and cathode catalysts, respectively. The cell was heated to 60 °C and the conductivity of the KOH was measured as 0.45 ± 0.1 S/cm. Carbon papers (Toray Industries, Japan) were used as gas diffusion layers. The carbon papers were spray-coated with the corresponding catalysts, using Nafion® (Nafion 117, ~5%, Sigma-Aldrich, Germany) as binder creating catalyst coated substrates which served as the electrodes. The flow plates were homemade from titanium and Au-coated. The potentials were recorded by a high-current potentiostat with implemented EIS module (Solartron Analytical, England). Before the EIS measurements, a break-in procedure was applied until the potential stabilized. EIS measurements were recorded in galvanostatic mode at current densities of 100 mA cm⁻², 250 mA cm⁻², 500 mA cm⁻², 750 mA cm⁻², and 1000 mA cm⁻². The current perturbation amplitude was set to 10% of the net applied current.

All EIS spectra were evaluated using the EIS Data Analysis 1.3 software.^[32,33]

Supporting Information

Supporting information is available.

Acknowledgements

This project has received funding from the European Union's Horizon 2020 research and innovation program under grant agreement HERMES No 952184. S.A.W. and R.M.K. want to express their thankfulness to the German Research Foundation (DFG) under Germany's excellence strategy – EXC 2089/1 –

390776260, Germany's excellence cluster "e-conversion", under DFG project BA 5795/6-1, and TUM IGSSE, project 11.01. Open Access funding enabled and organized by Projekt DEAL.

Conflict of Interests

The authors declare no conflict of interest.

Data Availability Statement

The data that support the findings of this study are available from the corresponding author upon reasonable request.

Keywords: anion exchange membrane electrolyzer · electrochemically active surface area · equivalent electrical circuit · impedance analysis · in-situ,

- [1] S. Griffiths, B. K. Sovacool, J. Kim, M. Bazilian, J. M. Uratani, *ERSS*. **2021**, *80*, 102208.
- [2] Y. Bai, Y. Momotani, M. C. Chen, A. Shibata, N. Tsuji, *Mater. Sci. Eng. A*. **2016**, *651*, 935–944.
- [3] M. D. Rashid, M. K. Al Mesfer, H. Naseem, M. Danish, *Int J Eng Adv Technol*. **2015**, *4*, 80–93.
- [4] M. R. Shaner, H. A. Atwater, N. S. Lewis, E. W. McFarland, *Energy Environ. Sci.* **2016**, *9*, 2354–2371.
- [5] N. Muradov, *Int. J. Hydrogen Energy*. **2017**, *42*, 14058–14088.
- [6] R. Guan, A. Wang, Y. Liang, J. Fu, X. Han, *Energies*. **2022**, *15*, 3573.
- [7] G. Di Bella, M. J. Flanagan, K. Foda, S. Maslova, A. Pienkowski, M. Stuermer, F. G. Toscani, *IMF Working Papers* **2022**, *145*.
- [8] D. W. Shin, M. D. Guiver, Y. M. Lee, *Chem. Rev.* **2017**, *117*, 4759–4805.
- [9] H. A. Miller, K. Bouzek, J. Hnat, S. Loos, C. I. Bernäcker, T. Weißgärber, L. Röntzsch, J. Meier-Haack, *Sustain. Energy Fuels*. **2020**, *4*, 2114–2133.
- [10] S. Ghoshal, B. S. Pivovar, S. M. Alia, *J. Power Sources* **2021**, *488*, 229433.
- [11] D. S. Falcão, A. M. F. R. Pinto, *J. Cleaner Prod.* **2020**, *261*, 121184.
- [12] C. Li, J. B. Baek, *Nano Energy* **2021**, *87*, 106162.
- [13] I. Vincent, E. C. Lee, H. M. Kim, *RSC Adv.* **2020**, *10*, 37429–37438.
- [14] I. Vincent, E. C. Lee, H. M. Kim, *Sci. Rep.* **2021**, *11*, 1–12.
- [15] A. K. Niaz, A. Akhtar, J. Y. Park, H. T. Lim, *J. Power Sources* **2021**, *481*, 229093.
- [16] Z. Zhao, S. Shi, H. Cao, Y. Li, *J. Membr. Sci.* **2017**, *530*, 220–231.
- [17] A. Lasia, *Electrochemical Impedance Spectroscopy and its Applications*, Springer-Verlag, New York **2014**, 367p.
- [18] S. Watzele, J. Fichtner, B. Garlyyev, J. N. Schwämmlein, A. S. Bandarenka, *ACS Catal.* **2018**, *8*, 9456–9462.5.
- [19] S. Back, K. Tran, Z. W. Ulissi, *ACS Catal.* **2019**, *9*, 7651–7659.
- [20] S. Watzele, A. S. Bandarenka, *Electroanalysis* **2016**, *28*, 2394–2399.
- [21] M. H. Aufa, S. A. Watzele, S. Hou, R. W. Haid, R. M. Kluge, A. S. Bandarenka, B. Garlyyev, *Electrochim. Acta* **2021**, *389*, 138692.
- [22] A. Ganassin, V. Colic, J. Tymoczko, A. S. Bandarenka, W. Schuhmann, *Phys. Chem. Chem. Phys.* **2015**, *17*, 8349–8355.
- [23] R. Kluge, R. Haid, A. S. Bandarenka, *J. Catal.* **2021**, *396*, 14–22.
- [24] M. Eikerling, A. A. Kornyshev, *JEAC* **1999**, *475*, 107–123.
- [25] A. Kosakian, University of Alberta **2021**.
- [26] A. Kosakian, M. Secanell, *Electrochim. Acta* **2021**, *367*, 137521.
- [27] T. Reshetenko, A. J. Kulikovskiy, *J. Electrochem. Soc.* **2018**, *165*, F291.
- [28] S. Touhami, J. Mainka, J. Dillet, S. A. H. Taleb, O. Lottin, *J. Electrochem. Soc.* **2019**, *166*, F1209.
- [29] S. M. Alia, B. Rasimick, et. al. *J. Electrochem. Soc.* **2016**, *163*, F3105.
- [30] https://www.heraeus.com/de/hpm/hmp_products_solutions/hydrogen_systems/catalysts_for_pem_electrolyzers/pem_electrolyzer_catalysts.html (accessed 07.26.2022).
- [31] S. Watzele, P. Hauenstein, Y. Liang, S. Xue, J. Fichtner, B. Garlyyev, D. Scieszka, F. Claudel, F. Maillard, A. S. Bandarenka, *ACS Catal.* **2019**, *9*, 9222–9230.
- [32] A. S. Bondarenko, *Anal. Chim. Acta*. **2012**, *743*.
- [33] A. S. Bandarenka, *Lecture Notes on Impedance Spectroscopy* **2013**, *4*, 29–36.

Manuscript received: July 3, 2023

Version of record online: January 12, 2024